






Induction of p16^{Ink4a} Gene Expression in Heme Protein–Induced AKI and by Heme: Pathophysiologic Implications

Karl A. Nath ¹, Raman Deep Singh ¹, Anthony J. Croatt,¹ Allan W. Ackerman,¹ Joseph P. Grande ¹, Daniel R. O'Brien,² Vesna D. Garovic ¹, Christopher M. Adams,³ Tamara Tchkonja,⁴ and James L. Kirkland ^{4,5}

Key Points

- In heme protein–mediated AKI (HP-AKI), a senescence phenotype promptly occurs, and increased expression of p16^{Ink4a} contributes to HP-AKI.
- Renal p16^{Ink4a} expression is induced by hemoglobin, myoglobin, and heme *in vivo* and in renal epithelial cells exposed to heme *in vitro*.
- Impairing the binding or degradation of heme by hemopexin deficiency or heme oxygenase-1 deficiency, respectively, further upregulates p16^{Ink4a}.

Abstract

Background Understanding the pathogenetic basis for AKI involves the study of ischemic and nephrotoxic models of AKI, the latter including heme protein–mediated AKI (HP-AKI). Recently, interest has grown regarding the role of senescence as a mechanism of kidney injury, including AKI. We examined whether senescence occurs in HP-AKI and potential inducers of and the role of a key driver of senescence, namely, p16^{Ink4a}, in HP-AKI.

Methods The long-established murine glycerol model of HP-AKI was used, and indices of senescence were examined. To evaluate the interaction of heme and p16^{Ink4a} expression, murine models of genetic deficiency of hemopexin (*HPX*) and heme oxygenase-1 (*HO-1*) were used. To determine the involvement of p16^{Ink4a} in HP-AKI, the population of p16^{Ink4a}-expressing cells was reduced using the *INK-ATTAC* model.

Results Using multiple indices, a senescence phenotype appears in the kidney within hours after the induction of HP-AKI. This phenotype includes significant upregulation of p16^{Ink4a}. p16^{Ink4a} is upregulated in the kidney after the individual administration of myoglobin, hemoglobin, and heme, as well as in renal epithelial cells exposed to heme *in vitro*. Genetic deficiencies of *HPX* and *HO-1*, which, independently, are expected to increase heme content in the kidney, exaggerate induction of p16^{Ink4a} in the kidney and exacerbate HP-AKI, the latter shown in the present studies involving *HPX*^{-/-} mice and in previous studies involving *HO-1*^{-/-} mice. Finally, reduction in the population of p16^{Ink4a}-expressing cells in the kidney improves renal function in HP-AKI even within 24 hours.

Conclusions The pathogenesis of HP-AKI involves senescence and the induction of p16^{Ink4a}, the latter driven, in part, by hemoglobin, myoglobin, and heme.

Kidney360 5: 501–514, 2024. doi: <https://doi.org/10.34067/KID.0000000000000395>

¹Division of Nephrology and Hypertension, Department of Medicine, Mayo Clinic, Rochester, Minnesota

²Division of Biomedical Statistics and Informatics, Department of Health Science Research, Mayo Clinic, Rochester, Minnesota

³Division of Endocrinology, Diabetes, Metabolism and Nutrition, Department of Medicine, Mayo Clinic, Rochester, Minnesota

⁴Department of Physiology and Biomedical Engineering, Mayo Clinic, Rochester, Minnesota

⁵Department of General Internal Medicine, Department of Medicine, Mayo Clinic, Rochester, Minnesota

Correspondence: Karl A. Nath, email: nath.karl@mayo.edu

Received: September 13, 2023 **Accepted:** February 5, 2024

Published Online Ahead of Print: February 21, 2024

Copyright © 2024 The Author(s). Published by Wolters Kluwer Health, Inc. on behalf of the American Society of Nephrology. This is an open access article distributed under the terms of the [Creative Commons Attribution-Non Commercial-No Derivatives License 4.0 \(CCBY-NC-ND\)](https://creativecommons.org/licenses/by-nc-nd/4.0/), where it is permissible to download and share the work provided it is properly cited. The work cannot be changed in any way or used commercially without permission from the journal.

Introduction

Occurring overall in some 10% of hospitalized patients, AKI may occur in excess of 50% of critically ill patients and may require RRT.^{1,2} The outcomes from AKI are influenced by age and the presence of age-related comorbidities, the nature and duration of the offending renal insult, the presence of CKD, the presence of systemic conditions including hypotension or sepsis, and whether AKI is part of a multisystem disease.^{1,2} The mortality from AKI may exceed 50%, and health care costs are vast (\$5.4–24.0 billion/yr).³ Patients who survive AKI may develop CKD and ESKD. Understanding the pathogenesis of AKI is vigorously pursued as such understanding may lead to novel therapies that mitigate the severity of AKI and/or promote renal regenerative and reparative processes.

The study of rodent models of AKI seeks to understand the pathogenesis of AKI.⁴ Such models include ischemia-reperfusion injury (IRI) and nephrotoxic injury, the latter encompassing heme protein-mediated AKI (HP-AKI), sepsis-associated AKI, and cisplatin-induced AKI. Our laboratory has focused on HP-AKI not only because of its relevance to AKI caused by rhabdomyolysis or hemolysis but also because AKI in sepsis or after cardiopulmonary bypass may be driven, in part, by cell-free hemoglobin.^{5–8} Moreover, in virtually all forms of AKI, kidney content of heme may increase because of destabilization of heme proteins (especially p450 cytochromes) in the injured kidney^{7,9,10}; this leads to the release of heme, the latter being a nephrotoxic and proinflammatory metabolite.⁷ Heme proteins may thus contribute to diverse types of AKI.^{7,8}

HP-AKI, induced by the intramuscular injection of hypertonic glycerol (which causes myolysis and hemolysis), has long and widely been studied by our and other laboratories.^{11,12} In this work, we explore the occurrence of senescence in HP-AKI. Senescence is a form of cell fate that predisposes to acute and chronic injury. The fundamental concept underlying senescence is that a specific cell type—the senescent cell (SC)—drives the pathobiology of senescence.^{13–15} SCs are cell cycle-arrested because of upregulation of either one or both of cell cycle inhibitors, p16^{Ink4a} and p21^{CIP1}; SCs are apoptosis-resistant because of upregulation of survival pathways. SCs exhibit the senescence associated secretory phenotype (SASP) which elaborates an array of proinflammatory cytokines, proteases, cytotoxic species, growth factors, and immune modulators.^{13–15} Largely through the SASP, senescence and SCs contribute to acute and chronic injury. In addition to the growing understanding of its pathobiology, the study of senescence led to strategies that may disrupt senescence, such as senolytics, the latter discovered by Zhu *et al.*¹⁶

Using diverse senescence markers, we assessed the occurrence of senescence in HP-AKI. We observed that the p16^{Ink4a} gene is markedly induced in murine HP-AKI and that heme itself induces p16^{Ink4a} gene and protein in human renal epithelial cells. To examine further the linkage among heme, p16^{Ink4a} expression, and renal injury, we examined the expression of p16^{Ink4a} when kidney heme content is predictably increased by either impaired heme-binding or impaired heme degradation in genetically altered mice; we found that such genetic deficiencies further increased p16^{Ink4a} expression. Finally, we assessed the functional significance of p16^{Ink4a} induction in HP-AKI.

Methods

In Vivo Studies

All studies were approved by the Institutional Animal Care and Use Committee of Mayo Clinic and performed in accordance with the Guide for the Care and Use of Laboratory Animals of the National Institutes of Health. Mice were housed in a temperature-controlled facility with 12-hour light-dark cycle, and food and water were provided *ad libitum*.

Mice

Male C57BL/6J mice (10–15 weeks old, Jackson Lab, Bar Harbor, ME) were used in studies involving the glycerol model of HP-AKI or the administration of hemoglobin, myoglobin, or hemin separately. In other studies, 11–17-week-old, age-matched male, hemopexin^{+/+} (HPX^{+/+}) and HPX^{-/-} mice were used in studies employing the glycerol model of HP-AKI.¹⁷ Similarly, 10–15-week-old, age-matched male and female heme oxygenase-1^{+/+} (HO-1^{+/+}) and heme oxygenase-1^{-/-} (HO-1^{-/-}) mice were also subjected to the glycerol model of HP-AKI.¹⁸ INK-ATTAC transgenic mice, developed by Kirkland, Tchkonja, and collaborators at Mayo Clinic were also subjected to the glycerol model of HP-AKI.¹⁹ INK-ATTAC female mice (14–15-month-old, generated and genotyped by the Kirkland laboratory) were randomized to two groups: (1) mice receiving intraperitoneal (IP) injection of vehicle (4% EtOH, 10% PEG-400, 86% Tween) or (2) mice receiving IP injection of AP20187 (10 mg/kg, in vehicle). AP20187 or vehicle was administered 30 minutes before and 6 hours after glycerol injection.

Model of Heme Protein-Mediated AKI (HP-AKI)

For the glycerol model of HP-AKI,^{20,21} mice were dehydrated overnight (16–18 hours) and, under ketamine and xylazine (90 and 10 mg/kg, respectively) anesthesia, an intramuscular injection of glycerol (50% in water), was performed, with one half of the dose given in each anterior thigh muscle. A glycerol dose of 6 ml/kg was used for studies at time points between 8 and 48 hours, and a 5 ml/kg dose was used for studies at 5 days. In addition, a dose of 7 ml/kg was used for studies in HPX^{+/+} and HPX^{-/-} mice at 4 days. Free access to water was restored after the injections. Kidneys and/or serum were harvested at time points ranging from 8 hours to 5 days after the glycerol injections.

IRI Model

The IRI model of AKI was used as in our previous study.²² Briefly, under pentobarbital (50 mg/kg, intraperitoneally) anesthesia, a midline abdominal incision was made, and each renal pedicle was gently dissected. Bilateral renal ischemia (22.5-minute duration) was induced using nontraumatic clamps (straight, 10 mm, 125 g pressure micro aneurysm clip, model no. RS5426, Roboz Surgical Instruments, Rockville, MD). One day after ischemia, kidneys were harvested for β -galactosidase (β -Gal) staining as described below. Sham procedures involved midline incision, but neither renal pedicle dissection nor clamping.

Administration of Heme Protein or Hemin In Vivo

Intravenous administration of hemoglobin or myoglobin (180 or 250 mg/100 g body weight, respectively, catalog nos. H2500 and M0630, Sigma Aldrich, St. Louis, MO) was

performed in C57BL/6J mice after 16–18 hours of dehydration. For these studies, kidney tissues were harvested for gene expression assessments 24 hours after these injections. In additional studies, hemin (hemin ferriprotoporphyrin IX chloride, 50 or 100 $\mu\text{mol/kg}$, IP) was administered to C57BL/6J mice at 6 and 24 hours before kidneys harvest.

Assessment of Renal Function

Plasma levels of BUN were measured using a commercially available kit (catalog no. B7551–120, Pointe Scientific, Canton, MI). Plasma creatinine was measured with a Creatinine Analyzer 2 (Beckman Instruments, Fullerton, CA).

In Vitro Studies

The human kidney proximal tubule cell line (HK-2) was obtained from ATCC (Manassas, VA) and used from passages 4–9. Briefly, these cells were maintained at 37°C in 95% air and 5% CO₂ in Keratinocyte Serum Free Medium (K-SFM, catalog no. 17005-042, ThermoFisher Scientific, Waltham, MA). In studies of heme exposure, HK-2 cells were incubated in DMEM (without phenol red) with 0.1% FBS containing hemin (20 or 25 μM , catalog no. H651-9, Frontier Scientific, Logan, UT) for 4, 6, and 16 hours. The cells were then harvested for the assessment of gene and protein expression as described.

Western Blot Analysis

Whole-kidney and cell lysates were subjected to western analysis as described in our previous studies.^{20,22} Membranes were incubated overnight at 4°C with primary antibodies against lamin B1 (catalog no. NBP2–67405; Novus Biologicals, Centennial, CO), hemopexin (catalog no. AF7007, R&D Systems, Minneapolis, MN), p16^{Ink4a} (catalog no. ab108349, Abcam, Waltham, MA); GAPDH (catalog no. 2118; Cell Signaling Technology, Danvers, MA), or β -actin (catalog no. 612656, BD Biosciences, Franklin Lakes, NJ). Membranes were then incubated with the appropriate HRP-conjugated secondary antibodies. Bands were visualized using enhanced chemiluminescence reagents.

Assessment of Gene Expression

mRNA expression was assessed in cells and whole-kidney tissues using a two-step quantitative real-time RT-PCR method as used in our previous studies.^{20,22} Briefly, RNA extraction was achieved using the TRIzol method (Invitrogen, Carlsbad, CA) with subsequent purification using a RNeasy Mini Kit (Qiagen, Valencia, CA). A Transcriptor First Strand cDNA Synthesis Kit (Roche Applied Science, Indianapolis, IN) was used for RT, and quantitative PCR was performed using TaqMan Gene Expression Assay sets (Applied Biosystems, Thermo Fisher Scientific) with standard curves constructed for the target and housekeeping genes. The results are reported as relative expression normalized to 18S rRNA.

Staining for β -Gal Activity

Staining for senescence-associated β -Gal activity was done on kidney slices using a modification of a method described in our previous studies.²³ Briefly, 1.5-mm thick cross-sectional slices of kidneys were fixed in 2% formaldehyde/0.2% glutaraldehyde in PBS for 10 minutes. The kidney slices were then incubated at 37°C in a staining solution (40 mM citric acid/sodium phosphate [pH 6.0],

5 mM potassium ferrocyanide, 5 mM potassium ferricyanide, 150 mM sodium chloride, 2 mM magnesium chloride, and 1 mg/ml 5-bromo-4-chloro-3-indolyl P3-d-galactoside). Color that developed after 4 hours of incubation was captured using a Nikon DS-Ri2 digital camera mounted on a Nikon SMZ800 stereo microscope.

Quantitative β -Gal Assay

Quantitative β -Gal activity measurements were made using the Senescence β -Gal Activity Assay Kit (Cell Signaling, cat. no. 23833). Kidney tissue homogenates were prepared in kit lysis buffer, and protein content was measured with the BCA reagent. 5 μg of total lysate was assayed in duplicate using a Fluoroskan plate reader (ThermoFisher Scientific) and reported as RFU/min per microgram protein.

RNA-In Situ Hybridization Staining

RNA-*in situ* hybridization (RNA-ISH) was performed using the standardized protocol for RNAscope 2.5 HD Assay-Brown assay from Advanced Cell Diagnostics, Inc. (Newark, CA). Briefly, kidney sections were deparaffinized, and antigen retrieval was performed as described in the kit. Sections were then processed for RNA-ISH per the manufacturer's protocol. Slides were finally counterstained with hematoxylin, and sections were mounted. Slides were imaged using an Olympus DP21 camera mounted on an Olympus BX60 microscope equipped with an UPlanFl 40 \times /0.75 lens. Images were acquired using CellSens software; exposure for all images was identical and processed identically using Photoshop.

Histology and Immunofluorescence Staining

Histologic examination was performed on formalin-fixed, paraffin-embedded kidney sections stained with hematoxylin and eosin. Semiquantitative assessment of histologic injury was based on a four-point scoring system that assessed epithelial cell necrosis and the degree of extension from the corticomedullary junction to the superficial cortex, cell sloughing, tubular dilatation, and cast formation.²⁴ Immunofluorescence staining was performed on 8- μm sections cut from formalin-fixed, paraffin-embedded kidney tissues.²² Briefly, slides were deparaffinized, and antigen retrieval with acidic citrate buffer (pH 6.0) was performed, blocked (5% normal donkey serum, 5% BSA in 0.1% Triton X-100, PBS) for 2 hours, and incubated with lamin-B1 primary antibody at 4°C overnight. Secondary antibody was incubated at room temperature, and slides were mounted using Vectashield mounting medium with DAPI (Vector Labs, Newark, CA) for nuclei staining. Microscope images (LSM780, Zeiss) were acquired using a 10 \times lens (NA 0.3), and images were prepared using Photoshop. All exposure levels and image processing were identical.

RNA Sequencing Analysis

RNA sequencing (RNASeq) analysis was performed as described.²³ Briefly, total RNA was extracted, and RNASeq was performed by Mayo Clinic's Medical Genome Facility. Genes with an average of ≥ 25 reads were processed for differential expression analysis. The R package edgeR²⁵ was used to identify which genes had a false discovery rate of < 0.05 with an absolute log₂ fold change of ≥ 2 from the group comparisons. The resulting differentially expressed genes' reads per kilobase per million mapped values were

then transferred to z-scores and used for a principal component analysis and unbiased hierarchical clustering with the ClustVis application.²⁶ Next, we performed a pathway analysis using kyota encyclopedia of gene genomes (KEGG) and an over-representation analysis using gene ontology (GO) by extracting the differentially expressed protein coding genes that exceeded an absolute log₂ fold change of ≥ 4 with a false discovery rate of <0.05 .²⁷ A total of 173 genes met our differentially expressed criteria. We used ShinyGO²⁷ to perform the enrichment analyses for the mouse KEGG pathways and mouse GO Biological Process terms. We also manually checked for enrichment of those differentially expressed genes in the GO Biological Process terms related to senescence.²⁸ We submitted the data to Geobank with the accession number GSE243366.

Statistics

Data are expressed as mean \pm SEM and considered statistically significant for $P < 0.05$. The Student *t* test was used for parametric data, and the Mann–Whitney *U* test was used for nonparametric data.

Results

Senescence and p16^{Ink4a} Induction after HP-AKI

Multiple indices indicate that renal senescence occurs after HP-AKI. β -Gal staining was robustly detected at 24 hours after HP-AKI (Figure 1A); by contrast, after acute ischemia reperfusion AKI, increased β -Gal staining was not observed after 24 hours (Supplemental Figure 1). Senescence was corroborated by the virtual disappearance of perinuclear staining of lamin B1 by immunofluorescence at this time point (Figure 1B), and even at 8 hours after HP-AKI, lamin B1 expression was reduced (Figure 1C); loss of lamin B1 is an established senescence marker.²⁹

We also assessed telomere erosion as another marker of senescence, using RNASeq analysis as described in our previous study.²³ Figure 2, A and B display the heat map and that fewer genes are expressed in HP-AKI within 1 MB of the telomeres. More than two-fold number of genes is lost within 1 MB of the telomeres in HP-AKI compared with the loss of genes not within 1 MB of the telomeres in HP-AKI, 9.86% versus 4.31%, $P = 0.00367$. These latter findings (telomere erosion) provide another marker of senescence. Additional analyses, shown in Figure 2, C and D, display the GO-biologic processes and KEGG pathway analyses, respectively. The high quality of these datasets is corroborated by data shown in Supplemental Figure 2, A–D and Supplemental Table 1.

In the GO and KEGG analyses of our RNASeq data, inflammatory pathways were quite significantly enriched. We thus examined RNA expression of specific components of the SASP 24 hours after HP-AKI. As shown in Table 1, a SASP was robustly upregulated at 24 hours after HP-AKI.

We proceeded to examine p16^{Ink4a} mRNA because this gene is one of the drivers of senescence. Significant induction of p16^{Ink4a} mRNA occurs in HP-AKI at 8 hours, and this persists through later time points, including 5 days (Figure 3A and Table 2). To determine the site of induction of p16^{Ink4a} in HP-AKI, we used RNA-ISH (RNA Scope) as is conventionally done, as commercially available antibodies do not reliably detect p16^{Ink4a} expression in murine tissue.

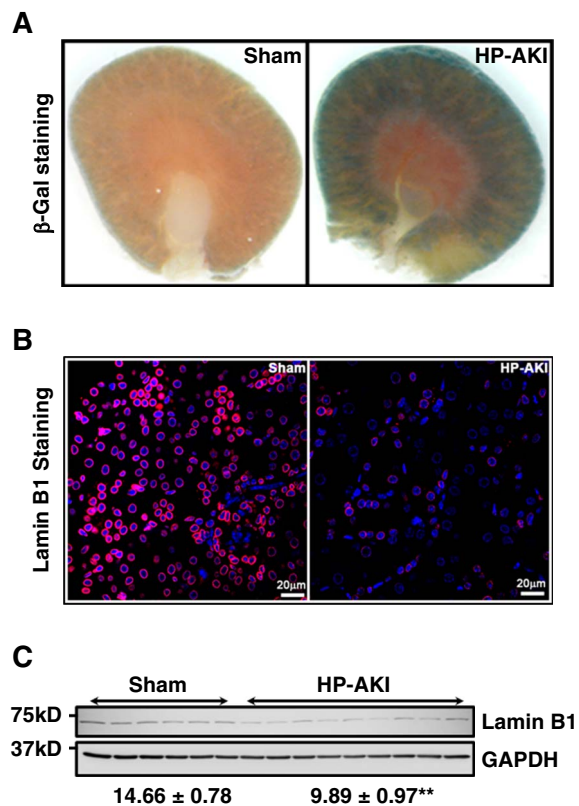


Figure 1. Markers of senescence after HP-AKI. (A) β -Gal staining in the kidney at 24 hours after HP-AKI. Prominent β -Gal staining is observed in the cortical and corticomedullary regions of the kidney after HP-AKI. (B) Lamin B1 expression in the kidney at 24 hours after HP-AKI. Immunofluorescence staining for nuclei (blue) and lamin B1 (red) in kidneys of mice 24 hours after sham (left panel) or HP-AKI (right panel). Lamin B1 expression in the perinuclear region of the cells in the cortex of mice kidneys is markedly reduced after HP-AKI. Scale bar = 20 μ m. (C) Western blot analysis of lamin B1 protein expression in the kidney 8 hours after HP-AKI. Lamin B1 expression in the kidneys of HP-AKI mice is significantly reduced. Equal protein loading is assessed by GAPDH immunoblotting. Normalized densitometric analysis for lamin B1 is displayed below the Western blots. $n=6$ and $n=9$ in sham and HP-AKI groups, respectively; ** $P < 0.01$ versus sham group. β -Gal, β -galactosidase.

p16^{Ink4a} mRNA induction largely localized to the proximal tubules of the kidney after HP-AKI (Figure 3B).

As p16^{Ink4a} mRNA was upregulated as far as the 5-day time point, we assessed additional markers of senescence at this time point. Components of the SASP were significantly upregulated, and β -Gal staining was increased in HP-AKI at the 5-day time point (Figure 4). In addition, at 5 days after HP-AKI, we measured renal β -Gal activity after HP-AKI; such activity was significantly increased compared with sham mice (642.55 ± 7.91 versus 914.27 ± 11.25 RFU/min per microgram of protein in sham versus HP-AKI groups, respectively, $n=5$ in each group).

We then determined when such senescence markers initially appeared after HP-AKI. After HP-AKI, β -Gal staining was weakly increased at 8 hours (Supplemental Figure 3) but robustly increased at 16 hours after HP-AKI (Supplemental Figure 4), the latter accompanied by a robustly expressed SASP (Table 2).

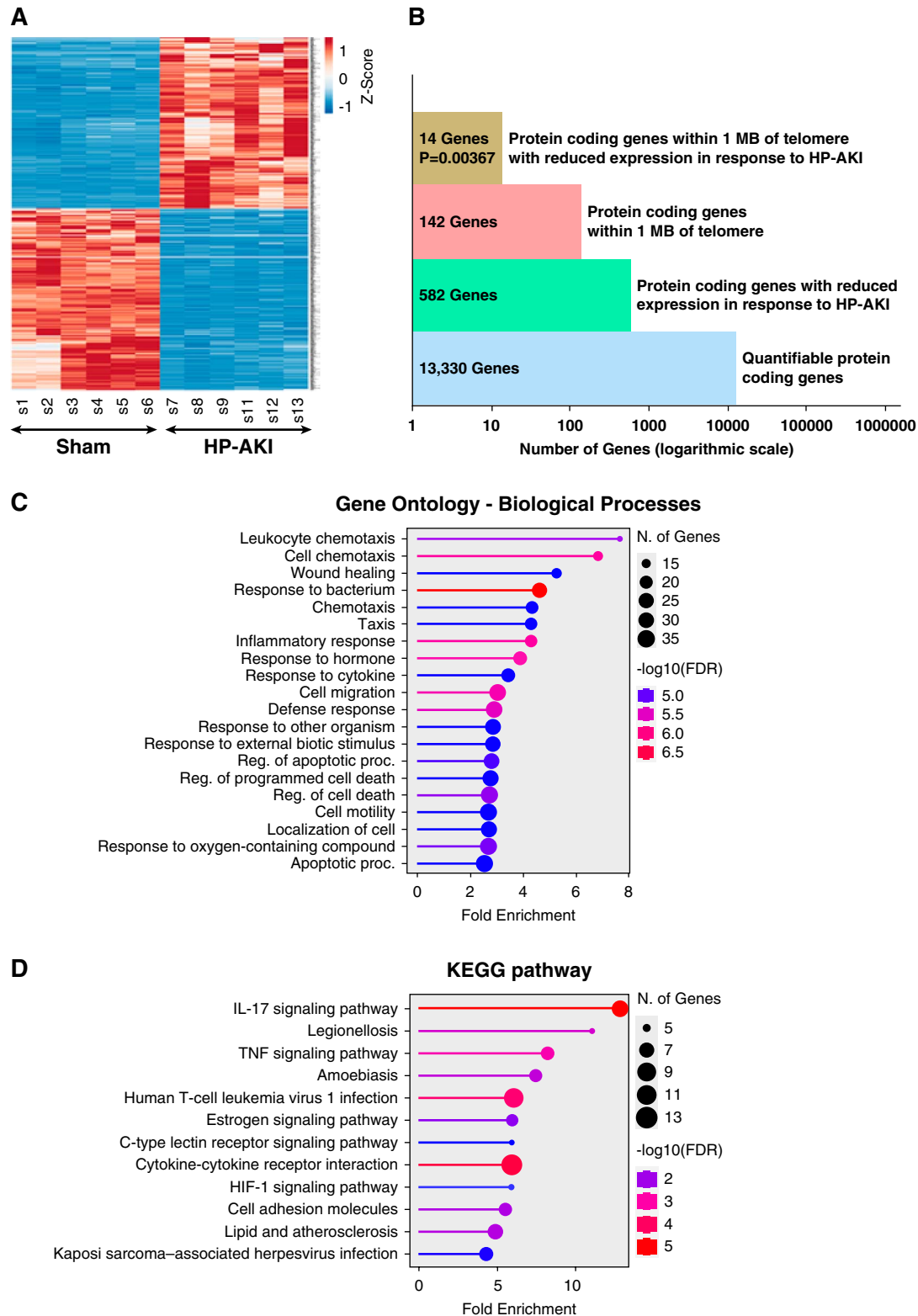


Figure 2. RNASeq analysis of gene expression in the kidney 24 hours after HP-AKI. (A) Heat map of genes differentially expressed in HP-AKI. Heat map analysis of genes with a false discovery rate of <0.05 and an absolute \log_2 fold change of ≥ 2 . (B) Telomere erosion. RNASeq analysis revealed reduced expression of genes in the 1 MB telomeric regions in the HP-AKI model (telomere erosion). In HP-AKI, the percent reduction of genes within the 1 MB telomeric regions was significantly greater than the percent reduction of genes not within the 1 MB of a telomeres (9.86% versus 4.31%, $P = 0.00367$). (C) Shiny GO and (D) KEGG analysis. This shows the fold enrichment, number of genes, and $-\log_{10}$ FDR of the GO terms and KEGG pathways enriched by the differentially expressed genes in several biological processes and pathways. GO, gene ontology; KEGG, kyota encyclopedia of gene genomes; RNASeq, RNA sequencing.

Table 1. Senescence-associated secretory phenotype gene expression in murine HP-AKI (24 hours)

Gene	Sham	HP-AKI	P Value
PAI-1	2.5±0.3	145.0±14.6	0.0079
CCL2	3.8±0.3	28.7±4.5	0.0079
IL-6	6.2±1.6	667.6±84.9	0.0079
TNF- α	10.3±0.9	21.9±2.7	0.0036
KC	6.2±0.9	285.6±58.3	0.0079

Real-time RT-PCR analysis normalized for 18S rRNA expression; $n=5$ each in sham and HP-AKI groups.

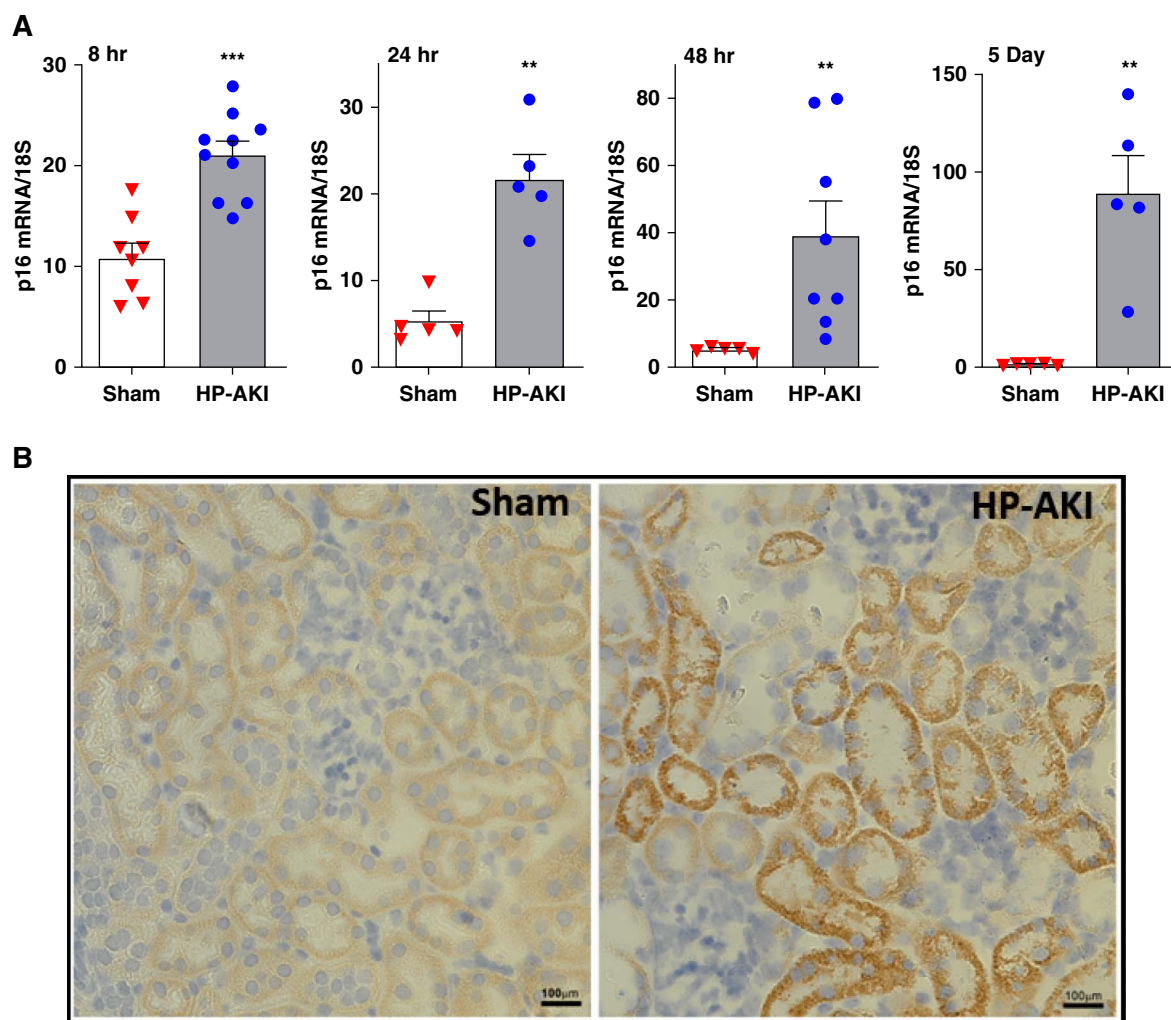


Figure 3. Expression of p16^{Ink4a} in the kidney after HP-AKI. (A) p16^{Ink4a} mRNA expression. p16^{Ink4a} mRNA expression in the kidneys of mice after HP-AKI is significantly increased compared with sham mice at 8 hours ($n=8$ and $n=10$ in sham and HP-AKI groups, respectively), 24 hours ($n=5$ in sham and HP-AKI groups), 48 hours ($n=5$ and $n=7$ in sham and HP-AKI groups, respectively), and 5 days ($n=5$ in each group). *** $P < 0.001$, ** $P < 0.01$ versus sham group. (B) Localization of p16^{Ink4a} mRNA expression in the kidney after HP-AKI using RNA-ISH. RNA-ISH staining shows increased p16^{Ink4a} expression in kidneys of HP-AKI mice at 24 hours. p16^{Ink4a} expression is induced in the proximal tubules of HP-AKI mice. Scale bar=100 μ m. RNA-ISH, RNA-*in situ* hybridization.

Heme Proteins and Heme Induce p16^{Ink4a}

Kidney content of hemoglobin, myoglobin, and heme is increased after HP-AKI. We determined whether these constituents induce p16^{Ink4a}. Twenty-four hours after administration of either constituent, p16^{Ink4a} mRNA was

induced by hemoglobin, myoglobin, or heme (Table 3). p16^{Ink4a} mRNA was also induced in human proximal tubular epithelial cells (HK-2 cells) exposed to heme for 4 or 6 hours (Figure 5A). At a later time, namely 16 hours of exposure to heme, p16^{Ink4a} protein expression was

Table 2. p16^{Ink4A} and senescence-associated secretory phenotype gene expression in murine HP-AKI (16 hours)

Gene	Sham	HP-AKI	P Value
p16	4.6±0.2	14.2±1.3	0.0079
PAI-1	1.3±0.1	57.4±2.0	0.0079
CCL2	3.9±0.6	14.8±1.0	<0.0001
IL-6	5.3±2.5	421.3±53.7	0.0079
TNF- α	3.4±0.3	6.1±1.1	0.0317
KC	9.5±3.7	173.7±42.2	0.0079

Real-time RT-PCR analysis normalized for 18S rRNA expression; n=5 each in sham and HP-AKI groups.

increased (Figure 5B); induction of p16^{Ink4a} protein was not apparent at earlier or later time points.

Studies in Hemopexin^{+/+} and Hemopexin^{-/-} Mice Subjected to HP-AKI

Hemopexin (HPX) is the major heme-binding protein ($K_D < 1$ pM). We hypothesize that mice genetically deficient in HPX (HPX^{-/-} mice) would be compromised in their heme-binding capacity, thereby leading to increased kidney content of free heme, upregulation of p16^{Ink4a} expression, and an exacerbation of HP-AKI. To examine this thesis, HPX^{+/+} and HPX^{-/-} mice were subjected to HP-AKI. Before this, we assessed whether HPX is induced in the kidney after HP-AKI. Expression of HPX mRNA and protein was significantly increased after HP-AKI compared with sham (Figure 6).

We then examined the sensitivity of the HPX-deficient kidney to HP-AKI (Table 4). By day 1 after HP-AKI, renal function was comparable between the two groups; by day 2, a tendency for worse kidney function appeared in HPX^{-/-} mice, and by days 3 and 4, renal function was significantly worse in HPX^{-/-} mice (Table 4). Histologic injury was also worse in HPX^{-/-} mice compared with HPX^{+/+} mice as evidenced by more marked epithelial cell necrosis and cortical extension, cell sloughing, and cast formation; HPX^{-/-} mice, but not HPX^{+/+} mice, after HP-AKI also exhibited dystrophic calcification, a finding indicative of severe histologic damage (Figure 7, A and B). The mean composite score for histologic injury was higher in HPX^{-/-} mice compared with HPX^{+/+} mice after HP-AKI (3.25±0.16 versus 2.00±0.27, $P = 0.0013$). No renal histologic abnormalities were present in either sham HPX^{+/+} or HPX^{-/-} mice. At the day 4 time point, p16^{Ink4a} mRNA was induced in both groups, but more markedly so in HPX^{-/-} mice after HP-AKI (Figure 7C). At the 4-day time point after HP-AKI, SASP components (PAI-1 and TNF- α) and an injury marker (KIM-1) were more prominently induced in HPX^{-/-} mice compared with HPX^{+/+} mice (Supplemental Figure 5).

Studies in HO-1^{+/+} and HO-1^{-/-} Mice Subjected to HP-AKI

Tissue levels of heme are controlled not only by binding to HPX but also by degradation by heme oxygenase (HO); inducible HO-1 is the predominant heme-degrading enzyme.^{30,31} To further examine the interaction among HP-AKI, heme, and p16^{Ink4a}, we used mice genetically deficient in HO-1, hypothesizing that impaired degradation

of heme in HO-1^{-/-} mice would increase free heme in the sham kidney and after HP-AKI, with augmentation in kidney p16^{Ink4a} mRNA expression. As shown in Table 5, under sham conditions, expression of p16^{Ink4a} mRNA was higher in HO-1^{-/-} mice compared with HO-1^{+/+} mice. However, the exaggerated p16^{Ink4a} induction hypothesized in HO-1^{-/-} mice subjected to HP-AKI compared with sham HO-1^{-/-} mice did not occur (Table 5). To explain this finding, we hypothesized that the absence of an HO-1-dependent pathway for heme removal would stimulate the heme-binding, HPX-based pathway as a compensatory response to mitigate the rise in free heme in the kidney. We thus assessed HPX mRNA in these mice. Indeed, after the instigation of HP-AKI, induction of HPX mRNA was 2.7-fold greater in HO-1^{-/-} mice compared with HO-1^{+/+} mice after HP-AKI (Table 5).

Studies in INK-ATTAC Mice Subjected to HP-AKI

INK-ATTAC mice are genetically altered mice such that p16^{Ink4a}-expressing cells in tissue can be removed. This is achieved by administering AP20187 which activates caspase 8, with apoptosis of p16^{Ink4a}-expressing cells.¹⁹ INK-ATTAC mice were treated with AP20187 or vehicle and then subjected to HP-AKI. Mice treated with AP20187, compared with vehicle-treated mice, exhibited less severe renal dysfunction as measured by serum creatinine and BUN (Figure 8). At this early time point after HP-AKI, we did not observe differences in renal histologic injury between AP20187-treated and vehicle-treated mice after HP-AKI.

Discussion

Senescence occurs relatively early after HP-AKI as evidenced by several indices: increased β -Gal activity, loss of lamin-B1 expression, telomere erosion, the appearance of a SASP, and p16^{Ink4a} upregulation. A senescence phenotype occurs in CKD and the AKI-CKD transition. A notable aspect of the present findings is how relatively early after HP-AKI a senescence phenotype appears (within 16 hours), unlike within days or weeks as described in other studies of AKI,³² the AKI-CKD transition,^{33,34} and CKD.³⁵ Instigation of a senescence phenotype is dependent on the nature and severity of the imposed stress. We thus identify acute exposure to HPs in the context of AKI as an inducer of the senescence phenotype. Dramatic alteration in gene expression (RNASeq studies) after HP-AKI attests to the severity of the imposed stress.

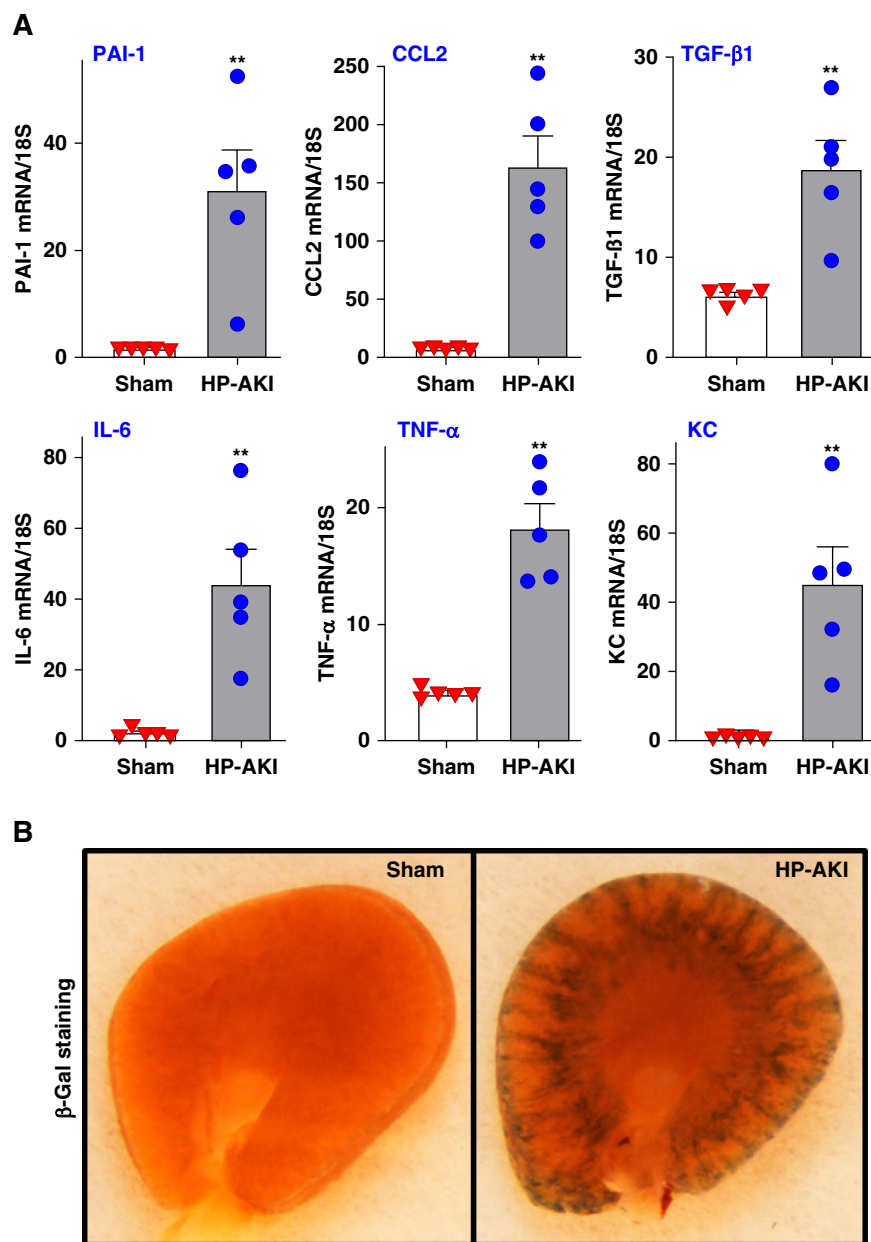


Figure 4. SASP expression and β -Gal staining in the kidney 5 days after HP-AKI. (A) SASP mRNA expression in the kidney 5 days after HP-AKI. Significantly increased mRNA expression of multiple SASP components was observed in the kidneys of mice 5 days after HP-AKI compared with sham mice ($n=5$ each in sham and HP-AKI groups). $**P < 0.01$ versus sham group. (B) β -Gal staining in the kidney 5 days after HP-AKI. Prominent β -Gal staining is observed in the cortical and corticomedullary regions of the kidney after HP-AKI. SASP, senescence-associated secretory phenotype.

Senescence is driven by $p16^{\text{Ink4a}}$, $p21^{\text{Cip1}}$, or both cyclin-dependent kinase inhibitors.^{13–15} We observed that $p16^{\text{Ink4a}}$ mRNA was induced by 8 hours after HP-AKI and persisted to the 5-day time point. Such mRNA expression was localized mainly to the proximal tubules, a major nephron segment injured by HP-AKI. The kidney in HP-AKI exhibits increased content of hemoglobin, myoglobin, and heme; all entities, individually, induced $p16^{\text{Ink4a}}$ mRNA *in vivo*; in addition, heme directly induces $p16^{\text{Ink4a}}$ mRNA and protein in proximal tubular epithelial cells. These studies are the first to identify heme proteins and heme as inducers of

$p16^{\text{Ink4a}}$ gene in the kidney. Previous studies demonstrate that RAW 264.7 macrophages exhibit $p16^{\text{Ink4a}}$ induction when HO-1 is knocked down and especially when these macrophages are also exposed to heme.³⁶ Knockdown of HO-1 is expected to increase cellular content of heme, as HO-1 is the predominant mechanism for degrading heme. Our studies reveal that, even without knockdown of HO-1, heme *per se* induces $p16^{\text{Ink4a}}$ mRNA and protein in renal proximal tubular epithelial cells. Notably, our previous studies demonstrate that heme reduces cell proliferation *in vitro* and thus elicits a consistent phenotype.³⁷

Table 3. Renal p16^{Ink4a} gene expression after the separate administration of hemoglobin, myoglobin, or hemin (24 hours)

Heme Protein or Hemin	Vehicle	Treatment
Hemoglobin	2.02±0.18	3.65±0.37 ^a
Myoglobin	2.52±0.29	4.34±0.44 ^b
Hemin		
50 μmol	2.89±0.26	4.11±0.32 ^b
100 μmol	1.15±0.21	2.33±0.24 ^b

Quantitative real-time RT-PCR normalized for 18S rRNA expression revealed significantly increased p16^{Ink4a} mRNA expression in the kidneys of mice separately treated (see Methods) with hemoglobin ($n=5$ in each group), myoglobin ($n=4$ in each group), hemin 50 μmol/kg body weight ($n=4$ and $n=5$ in vehicle and hemin treated groups), and hemin 100 μmol/kg body weight ($n=5$ in each group).

^a $P < 0.01$ versus relevant vehicle.

^b $P < 0.05$ versus relevant vehicle.

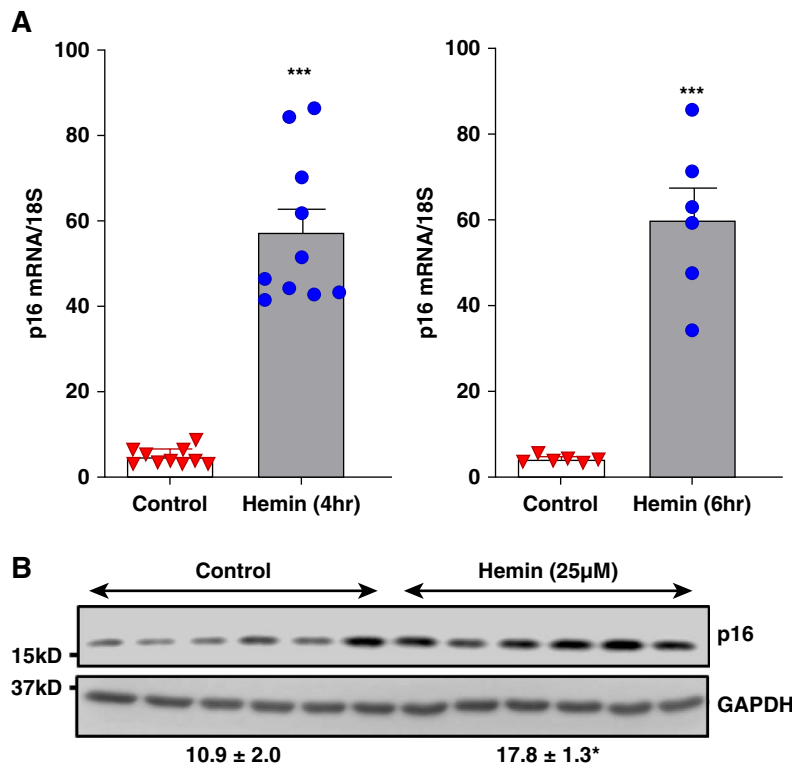


Figure 5. p16^{Ink4a} expression in hemin-treated HK-2 cells. (A) p16^{Ink4a} mRNA expression. p16^{Ink4a} mRNA expression is significantly increased in hemin-treated (20 μM) HK-2 cells at 4 hours ($n=10$ in each group) and 6 hours ($n=6$ in each group). *** $P < 0.001$ versus control cells. (B) p16^{Ink4a} protein expression. Western blot analysis of p16^{Ink4a} protein expression in control and hemin-treated (25 μM) HK-2 cells shows significantly increased p16^{Ink4a} protein expression at 16 hours of hemin treatment. Equal protein loading is assessed by GAPDH immunoblotting. Normalized densitometric analysis for p16^{Ink4a} is shown below the Western blot. * $P < 0.05$ versus control cells.

Our finding that heme induces p16^{Ink4a} expression leads us to offer two speculations. First, heme-driven p16^{Ink4a} induction may be one of the common pathways of p16^{Ink4a} upregulation in tissue injury as in injured cells, intracellular heme proteins, particularly, cytochrome p450 heme proteins, may be destabilized leading to increased intracellular content of free heme.^{7,9,10} Second, hemolytic diseases, such as sickle cell disease, are attended by increased plasma and intracellular levels of heme³⁸; preeclampsia of pregnancy, a hemolytic condition, is associated with a senescence phenotype.³⁹ On the basis of the senescence phenotype we

observed in HP-AKI (induced by myolysis and hemolysis), we speculate that senescence may occur in other hemolytic conditions.

To analyze further the association among HP-AKI, heme, and p16^{Ink4a}, we examined the HP-AKI model in *HPX*^{+/+} and *HPX*^{-/-} mice. Our findings demonstrate in a *bone fide* model of HP-AKI that the genetic deficiency of *HPX* worsens renal function and histologic injury. Moreover, in kidneys deficient in heme-binding capacity (because of the absence of *HPX*), and, predictably, with higher heme content after HP-AKI, p16^{Ink4a} mRNA induction was

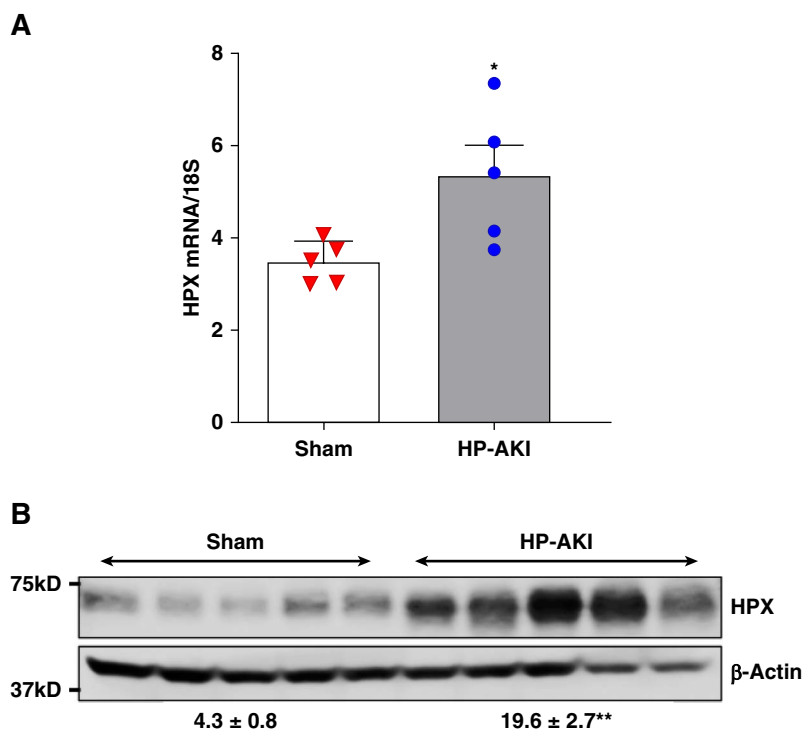


Figure 6. Hemopexin expression in the kidney after HP-AKI. (A) HPX mRNA expression. Renal HPX mRNA expression is significantly increased at 24 hours after HP-AKI compared with sham ($n=5$ in sham and HP-AKI groups). (B) Western blot analysis after HP-AKI. Western blot analysis shows significantly increased HPX protein expression at 24 hours in HP-AKI mice compared with sham mice ($n=5$ in sham and HP-AKI groups). Protein loading is evaluated by β -actin immunoblotting. Normalized densitometric analysis for HPX protein is shown below the western blots. $**P < 0.01$, $*P < 0.05$ versus sham group. HPX, hemopexin.

Table 4. Renal filtration markers in $HPX^{+/+}$ and $HPX^{-/-}$ mice at days 1–4 after HP-AKI

Time Point	Serum Creatinine (mg/dl)		BUN (mg/dl)	
	$HPX^{+/+}$	$HPX^{-/-}$	$HPX^{+/+}$	$HPX^{-/-}$
1D	1.59 \pm 0.14	1.67 \pm 0.14	136.2 \pm 8.7	146.0 \pm 5.4
2D	1.30 \pm 0.11	1.66 \pm 0.22	126.4 \pm 18.8	160.6 \pm 13.0
3D	0.82 \pm 0.11	1.38 \pm 0.20 ^a	104.8 \pm 16.9	166.3 \pm 23.6 ^a
4D	0.66 \pm 0.08	1.21 \pm 0.20 ^b	81.7 \pm 10.8	142.0 \pm 23.4 ^a

Significantly increased levels of both serum creatinine and BUN levels were observed on day 3 (3D) and day 4 (4D) after HP-AKI. Values are mean \pm SEM; $n=8$ each in $HPX^{+/+}$ and $HPX^{-/-}$ mice.
^a $P < 0.05$ versus $HPX^{+/+}$ for that day.
^b $P < 0.01$ versus $HPX^{+/+}$ for that day.

exaggerated in $HPX^{-/-}$ mice compared with $HPX^{+/+}$ mice after HP-AKI. These findings are consistent with the linkage between heme content and induction of p16^{Ink4a} mRNA. However, it is possible that HPX may contribute other effects besides heme binding, relevant to the sensitivity of $HPX^{-/-}$ mice to HP-AKI.

Previous studies using the oxidant phenylhydrazine to induce hemolysis failed to assess renal function but did observe worse renal histologic injury in phenylhydrazine-treated $HPX^{-/-}$ mice.⁴⁰ An added consideration is that because of the oxidizing capacity of phenylhydrazine, it is unclear whether the exacerbatory effect of genetic

deficiency of HPX reflects an impaired antioxidant capability rather than impaired heme binding. Our present studies also support the increasing interest in the potential tissue-protecting effect of HPX when tissues are exposed to an increased burden of heme proteins, as occurs in sickle cell disease and in other hemolytic states.⁴¹ Finally, a recent study demonstrated that $HPX^{-/-}$ mice, compared with $HPX^{+/+}$ mice, had less AKI when subjected to IRI and cisplatin AKI (CP-AKI); these studies noted that HPX accumulates in the kidney in both IRI and CP-AKI.⁴² This study concluded that in IRI and CP-AKI, HPX induces AKI by promoting renal accumulation of hemoglobin and iron-

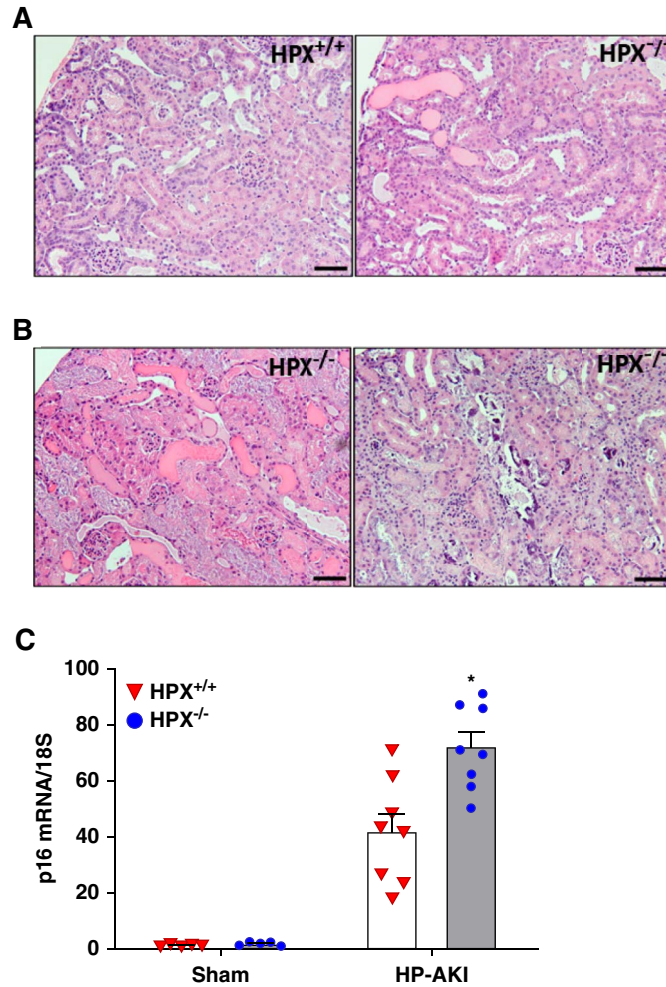


Figure 7. Histological analysis of the kidney in $HPX^{+/+}$ and $HPX^{-/-}$ mice at 4 days after HP-AKI. (A) Histologic sections of the kidney in $HPX^{+/+}$ and $HPX^{-/-}$ mice after HP-AKI. Cell necrosis, sloughing, and cast formation are more severe in $HPX^{-/-}$ mice (right panel) compared with $HPX^{+/+}$ mice (left panel). Scale bar=100 μm . (B) Distinct histologic features in $HPX^{-/-}$ mice subjected to HP-AKI. This shows the severity of histologic lesions (left panel) and the presence of dystrophic calcification (right panel) that occur in some $HPX^{-/-}$ mice, neither of which occurs in $HPX^{+/+}$ mice subjected to HP-AKI. Scale bar=100 μm . (C) p16^{Ink4a} mRNA expression in the kidney of $HPX^{+/+}$ and $HPX^{-/-}$ mice at 4 days after HP-AKI. Such expression is increased in the kidneys of $HPX^{-/-}$ mice compared with $HPX^{+/+}$ mice. $n=5$ each in sham groups and $n=8$ each in HP-AKI groups. * $P < 0.01$ in $HPX^{-/-}$ mouse kidneys versus $HPX^{+/+}$ mouse kidneys after HP-AKI.

Table 5. Renal p16^{Ink4a} and hemopexin gene expression in $HO-1^{+/+}$ and $HO-1^{-/-}$ mice after HP-AKI

Treatment	Renal p16 Expression		Renal HPX Expression	
	$HO-1^{+/+}$	$HO-1^{-/-}$	$HO-1^{+/+}$	$HO-1^{-/-}$
Sham	7.82±0.84	16.87±2.64 ^a	8.19±3.65	19.78±6.48
HP-AKI	11.07±0.65	17.04±1.37 ^b	29.99±11.07	82.09±14.70 ^a

Quantitative real-time RT-PCR of p16^{Ink4a} and hemopexin mRNA expression at 24 hours after sham or HP-AKI treatment, normalized for 18S rRNA expression. $n=8$ in each sham treated group, and $n=12$ and $n=13$ in $HO-1^{+/+}$ and $HO-1^{-/-}$ HP-AKI treated groups, respectively. HO, heme oxygenase; HPX, hemopexin.

^a $P < 0.05$ versus $HO-1^{+/+}$ group for that treatment.

^b $P < 0.01$ versus $HO-1^{+/+}$ group for that treatment.

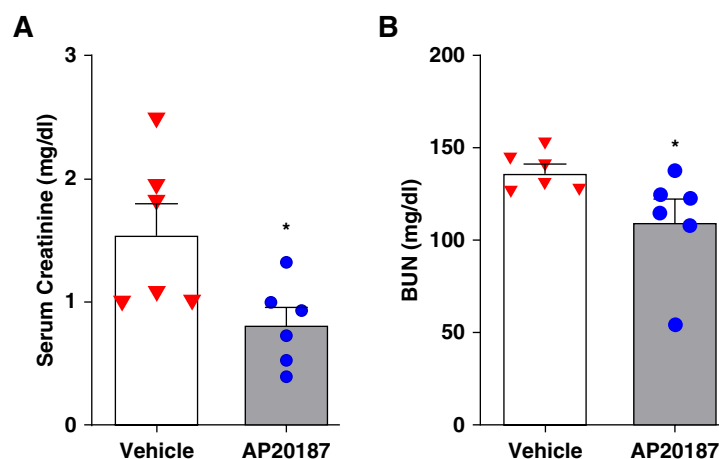


Figure 8. Renal function after HP-AKI in *INK-ATTAC* mice in which p16^{Ink4a}-overexpressing cells are reduced by AP20187. (A) Serum creatinine 24 hours after HP-AKI. (B) BUN levels 24 hours after HP-AKI. Both filtration markers are significantly decreased with the administration of AP20187 compared with such filtration markers with vehicle treatment. $n=6$ in each group. $*P < 0.05$ versus vehicle.

driven AKI.⁴² Our studies show that in an established model of HP-AKI, the genetic deficiency of HPX promotes AKI, assessed by functional markers, histologic injury, and injury biomarkers. Thus, the behavior of HPX—be it a protectant or perpetrator in AKI—is dependent on the specific cause of AKI.

To further examine the interaction among HP-AKI, heme, and p16^{Ink4a}, we used mice deficient in HO-1 and thus profoundly compromised in heme-degrading capacity. In the unstressed, basal state, *HO-1*^{-/-} mice exhibited increased p16^{Ink4a} mRNA expression, which may reflect the inductive effect of higher ambient levels of heme when HO-1 is deficient. However, to our surprise, when *HO-1*^{+/+} and *HO-1*^{-/-} mice are stressed with HP-AKI, an exaggerated induction of p16^{Ink4a} mRNA failed to occur in *HO-1*^{-/-} mice. To account for this observation, we assessed HPX mRNA expression and observed that induction was accentuated in *HO-1*^{-/-} mice compared with *HO-1*^{+/+} mice after HP-AKI. We suggest that this accentuated HPX induction in *HO-1*^{-/-} kidneys after HP-AKI provides enhanced heme-binding capability; this mitigates the rise in free heme that would otherwise occur because of the loss of heme-degrading capacity. We are unaware of such findings in the kidney that demonstrate, in response to a HP burden, adaptive increments in renal HPX mRNA expression compensate for *HO-1* deficiency.

To examine the role of p16^{Ink4a} in HP-AKI, we examined the effect of depleting p16^{Ink4a}-expressing cells in HP-AKI. We used the *INK-ATTAC* strategy that reduces the population of p16^{Ink4a}-expressing cells by inducing apoptosis of these cells. At 24 hours after HP-AKI, such reduction in p16^{Ink4a}-expressing cells was attended by less severe HP-AKI as reflected by two filtration markers. Thus, induction of p16^{Ink4a} contributes to HP-AKI as renal function is improved when p16^{Ink4a}-expressing cells are reduced in number. We offer the following considerations in interpreting these findings. First, the bulk of studies that used the *INK-ATTAC* strategy to reduce p16^{Ink4a}-expressing cells has been in chronic injury where the precipitancy and severity of tissue injury are less than in acute tissue injury^{13–15}; it is thus

notable that even with acute injury of this severity as the HP-AKI model, this strategy implicates a pathogenetic involvement of p16^{Ink4a}. Second, the time point studied was relatively early after HP-AKI; it is conceivable that more dramatic effects including less histologic injury may be observed at later time points; this indeed was the case with previous studies of *HO-1*^{-/-} and *HO-1*^{+/+} mice (HO-1 is one of most potent protectants in HP-AKI) in which no significant differences were observed on day 1 after HP-AKI, but significantly higher serum creatinine appeared in *HO-1*^{-/-} mice thereafter²¹; similarly, in the present *HPX*^{-/-} studies in response to HP-AKI, worse renal function emerged on days 3 and 4 in *HPX*^{-/-} mice. Third, not all p16^{Ink4a}-expressing cells may be deleted by the *INK-ATTAC* strategy and thus less AKI occurred although not all such cells were depleted; assessment of the depletion of p16^{Ink4a}-expressing cells and senescence would thus be of interest. Fourth, p16^{Ink4a} contributes to the senescence phenotype that includes a SASP; we thus speculate that the beneficial effects of reducing p16^{Ink4a}-expressing cells in HP-AKI arise from less inflammation.^{7,20} Studies of compounds that modulate the activity of cyclin dependent kinase inhibitors are of interest.

In summary, we demonstrate that a senescence phenotype appears within 16 hours in the kidney after HP-AKI. This phenotype includes significant upregulation of p16^{Ink4a} mRNA. p16^{Ink4a} mRNA is induced in the kidney when myoglobin, hemoglobin, and heme are separately administered *in vivo*, as well as renal epithelial cells exposed to heme *in vitro*. Genetic deficiencies of *HPX* or *HO-1*, which, independently, are predicted to increase kidney heme content, exaggerate the induction of p16^{Ink4a} mRNA in the kidney. Finally, depleting p16^{Ink4a}-expressing cells improves renal function in HP-AKI at 24 hours.

Disclosures

C.M. Adams reports the following: Ownership Interest: Emmyon, Inc.; Research Funding: Emmyon, Inc.; Patents or Royalties: Emmyon, Inc.; and Advisory or Leadership Role: Emmyon, Inc. V.D. Garovic reports the following: Patents or Royalties: I am

the inventor of the technology “Markers for preeclampsia.” The technology has not been licensed. J.P. Grande reports the following: Advisory or Leadership Role: Member of the Editorial Board for *Biochemistry and Molecular Biology Education* Journal, Not paid. J.L. Kirkland and T. Tchkonja have a financial interest related to this research, including patents and pending patents covering senolytic drugs and their uses that are held by Mayo Clinic. This research has been reviewed by the Mayo Clinic Conflict of Interest Review Board and was conducted in compliance with Mayo Clinic conflict of interest policies. J.L. Kirkland reports the following: Ownership Interest: Unity Biotechnology; Honoraria: AbbVie Inc.; and Patents or Royalties: Unity Biotechnology. K.A. Nath reports the following: Advisory or Leadership Role: Former Editor-in-Chief, *JASN*. T. Tchkonja reports the following: Ownership Interest: Unity Biotechnology Inc.; Honoraria: HRI Roswell Park Division, Buffalo, NY and Pfizer; and Patents or Royalties: UNITY Biotechnology; Mayo Clinic holds patents related to senolytics and animal models for studying senescent cells. All remaining authors have nothing to disclose.

Funding

K.A. Nath: National Institute of Diabetes and Digestive and Kidney Diseases (R01 DK133401 and R01 DK119167). C.M. Adams: National Institute on Aging (R01 AG060637). V.D. Garovic: National Heart, Lung, and Blood Institute (R01 HL136348). J.L. Kirkland: National Institute on Aging (R37AG013925), The Connor Fund, Robert J. and Theresa W. Ryan, and Noaber Foundation.

Acknowledgment

We are grateful to Dr. Ray F. Regan for kindly providing mice to establish a colony used to generate *HPX^{+/+}* and *HPX^{-/-}* mice used in this study.

Author Contributions

Conceptualization: Christopher M. Adams, Anthony J. Croatt, Joseph P. Grande, James L. Kirkland, Karl A. Nath, Raman Deep Singh.

Data curation: Allan W. Ackerman, Anthony J. Croatt, Joseph P. Grande, Karl A. Nath, Daniel R. O'Brien, Raman Deep Singh.

Formal analysis: Allan W. Ackerman, Christopher M. Adams, Anthony J. Croatt, Joseph P. Grande, James L. Kirkland, Karl A. Nath, Daniel R. O'Brien, Raman Deep Singh.

Funding acquisition: Karl A. Nath.

Investigation: Allan W. Ackerman, Anthony J. Croatt, Karl A. Nath, Raman Deep Singh.

Methodology: Anthony J. Croatt, Karl A. Nath, Raman Deep Singh.

Project administration: Anthony J. Croatt, Karl A. Nath.

Resources: Anthony J. Croatt, Karl A. Nath, Raman Deep Singh.

Software: Allan W. Ackerman, Anthony J. Croatt, Daniel R. O'Brien, Raman Deep Singh.

Supervision: Anthony J. Croatt, Karl A. Nath, Raman Deep Singh.

Validation: Allan W. Ackerman, Anthony J. Croatt, Vesna D. Garovic, Joseph P. Grande, Karl A. Nath, Daniel R. O'Brien, Raman Deep Singh.

Visualization: Anthony J. Croatt, Karl A. Nath, Raman Deep Singh.

Writing – original draft: Allan W. Ackerman, Anthony J. Croatt, Joseph P. Grande, Karl A. Nath, Daniel R. O'Brien, Raman Deep Singh.

Writing – review & editing: Allan W. Ackerman, Christopher M. Adams, Anthony J. Croatt, Vesna D. Garovic, Joseph P. Grande, James L. Kirkland, Karl A. Nath, Daniel R. O'Brien, Raman Deep Singh, Tamara Tchkonja.

Data Sharing Statement

All data are included in the manuscript and/or supporting information. RNAseq data deposited to Geobank, accession number GSE243366.

Supplemental Material

This article contains the following supplemental material online at <http://links.lww.com/KN9/A445>.

Supplemental Figure 1. Senescence assessed in the kidney after ischemia reperfusion injury (IRI) at 24 hours using β -galactosidase (β -gal) staining of kidneys. Increased β -galactosidase staining was not detected in the kidney after IRI.

Supplemental Figure 2. The high quality of these datasets is shown with mapping percentages indicating that the reads from all samples are uniquely mapping to expressed RNA features. High mapping percentages and consistency across every category and in all samples without 3' or 5' coverage biases are indicative of high-quality RNASeq data.

Supplemental Table 1. No samples were seen with inconsistent alignment metrics indicating that our data can be reliably used to perform the analyses conducted in this study for investigating the legitimate transcriptomic differences between our groups of samples.

Supplemental Figure 3. Senescence assessed in the kidney at 8 hours after HP-AKI using β -galactosidase staining of the kidney. Faint β -galactosidase staining at 8 hours after HP-AKI was observed when compared with sham kidney.

Supplemental Figure 4. Senescence assessed in the kidney at 16 hours after HP-AKI using β -galactosidase staining of the kidney. Pronounced differences in β -gal staining were observed at 16 hours after HP-AKI compared with sham kidney.

Supplemental Figure 5. mRNA expression of SASP components (TNF- α and PAI-1) and an injury marker (KIM-1) at 4 days after HP-AKI in the kidneys of *HPX^{+/+}* and *HPX^{-/-}* mice. Significantly increased mRNA expression of SASP components and KIM-1 was observed after HP-AKI compared with sham mice ($n=5$ and $n=8$ in each sham and HP-AKI group, respectively). *** $P < 0.001$ and * $P < 0.05$ versus sham group.

References

- Agarwal A, Dong Z, Harris R, et al.; Acute Dialysis Quality Initiative XIII Working Group. Cellular and molecular mechanisms of AKI. *J Am Soc Nephrol*. 2016;27(5):1288–1299. doi:10.1681/ASN.2015070740
- Zuk A, Bonventre JV. Acute kidney injury. *Annu Rev Med*. 2016;67:293–307. doi:10.1146/annurev-med-050214-013407
- Silver SA, Chertow GM. The economic consequences of acute kidney injury. *Nephron*. 2017;137(4):297–301. doi:10.1159/000475607
- Nath KA. Models of human AKI: resemblance, reproducibility, and return on investment. *J Am Soc Nephrol*. 2015;26(12):2891–2893. doi:10.1681/ASN.2015101109
- Haase M, Haase-Fielitz A, Bagshaw SM, Ronco C, Bellomo R. Cardiopulmonary bypass-associated acute kidney injury: a pigment nephropathy? *Contrib Nephrol*. 2007;156:340–353. doi:10.1159/000102125
- Kerchberger VE, Ware LB. The role of circulating cell-free hemoglobin in sepsis-associated acute kidney injury. *Semin Nephrol*. 2020;40(2):148–159. doi:10.1016/j.semnephrol.2020.01.006
- Nath KA, Singh RD, Croatt AJ, Adams CM. Heme proteins and kidney injury: beyond rhabdomyolysis. *Kidney360*. 2022;3(11):1969–1979. doi:10.34067/kid.0005442022
- Westenfelder C, Gooch A. Heme protein-induced acute kidney injury is caused by disruption of mitochondrial homeostasis in

- proximal tubular cells. *Kidney360*. 2022;3(12):2140–2142. doi: [10.34067/kid.0006372022](https://doi.org/10.34067/kid.0006372022)
9. Paller MS, Jacob HS. Cytochrome P-450 mediates tissue-damaging hydroxyl radical formation during reoxygenation of the kidney. *Proc Natl Acad Sci U S A*. 1994;91(15):7002–7006. doi: [10.1073/pnas.91.15.7002](https://doi.org/10.1073/pnas.91.15.7002)
 10. Liu H, Baliga R. Cytochrome P450 2E1 null mice provide novel protection against cisplatin-induced nephrotoxicity and apoptosis. *Kidney Int*. 2003;63(5):1687–1696. doi: [10.1046/j.1523-1755.2003.00908.x](https://doi.org/10.1046/j.1523-1755.2003.00908.x)
 11. Nath KA, Balla G, Vercellotti GM, et al. Induction of heme oxygenase is a rapid, protective response in rhabdomyolysis in the rat. *J Clin Invest*. 1992;90(1):267–270. doi: [10.1172/jci115847](https://doi.org/10.1172/jci115847)
 12. Westenfelder C, Arevalo GJ, Crawford PW, et al. Renal tubular function in glycerol-induced acute renal failure. *Kidney Int*. 1980;18(4):432–444. doi: [10.1038/ki.1980.156](https://doi.org/10.1038/ki.1980.156)
 13. Kirkland JL, Tchkonja T. Senolytic drugs: from discovery to translation. *J Intern Med*. 2020;288(5):518–536. doi: [10.1111/joim.13141](https://doi.org/10.1111/joim.13141)
 14. Pignolo RJ, Passos JF, Khosla S, Tchkonja T, Kirkland JL. Reducing senescent cell burden in aging and disease. *Trends Mol Med*. 2020;26(7):630–638. doi: [10.1016/j.molmed.2020.03.005](https://doi.org/10.1016/j.molmed.2020.03.005)
 15. Chaib S, Tchkonja T, Kirkland JL. Cellular senescence and senolytics: the path to the clinic. *Nat Med*. 2022;28(8):1556–1568. doi: [10.1038/s41591-022-01923-y](https://doi.org/10.1038/s41591-022-01923-y)
 16. Zhu Y, Tchkonja T, Pirtskhalava T, et al. The Achilles' heel of senescent cells: from transcriptome to senolytic drugs. *Aging Cell*. 2015;14(4):644–658. doi: [10.1111/acer.12344](https://doi.org/10.1111/acer.12344)
 17. Nath KA, Grande JP, Belcher JD, et al. Antithrombotic effects of heme-degrading and heme-binding proteins. *Am J Physiol Heart Circ Physiol*. 2020;318(3):H671–H681. doi: [10.1152/ajpheart.00280.2019](https://doi.org/10.1152/ajpheart.00280.2019)
 18. Nath KA, Vercellotti GM, Grande JP, et al. Heme protein-induced chronic renal inflammation: suppressive effect of induced heme oxygenase-1. *Kidney Int*. 2001;59(1):106–117. doi: [10.1046/j.1523-1755.2001.00471.x](https://doi.org/10.1046/j.1523-1755.2001.00471.x)
 19. Baker DJ, Wijshake T, Tchkonja T, et al. Clearance of p16Ink4a-positive senescent cells delays ageing-associated disorders. *Nature*. 2011;479(7372):232–236. doi: [10.1038/nature10600](https://doi.org/10.1038/nature10600)
 20. Singh RD, Croatt AJ, Ackerman AW, et al. Prominent mitochondrial injury as an early event in heme protein-induced acute kidney injury. *Kidney360*. 2022;3(10):1672–1682. doi: [10.34067/kid.0004832022](https://doi.org/10.34067/kid.0004832022)
 21. Nath KA, Haggard JJ, Croatt AJ, Grande JP, Poss KD, Alam J. The indispensability of heme oxygenase-1 in protecting against acute heme protein-induced toxicity in vivo. *Am J Pathol*. 2000;156(5):1527–1535. doi: [10.1016/s0002-9440\(10\)65024-9](https://doi.org/10.1016/s0002-9440(10)65024-9)
 22. Nath KA, Singh RD, Grande JP, et al. Expression of ACE2 in the intact and acutely injured kidney. *Kidney360*. 2021;2(7):1095–1106. doi: [10.34067/kid.0001562021](https://doi.org/10.34067/kid.0001562021)
 23. Nath KA, O'Brien DR, Croatt AJ, et al. The murine dialysis fistula model exhibits a senescence phenotype: pathobiological mechanisms and therapeutic potential. *Am J Physiol Renal Physiol*. 2018;315(5):F1493–F1499. doi: [10.1152/ajprenal.00308.2018](https://doi.org/10.1152/ajprenal.00308.2018)
 24. Nath KA, Croatt AJ, Warner GM, Grande JP. Genetic deficiency of Smad3 protects against murine ischemic acute kidney injury. *Am J Physiol Renal Physiol*. 2011;301(2):F436–F442. doi: [10.1152/ajprenal.00162.2011](https://doi.org/10.1152/ajprenal.00162.2011)
 25. Robinson MD, McCarthy DJ, Smyth GK. edgeR: a Bioconductor package for differential expression analysis of digital gene expression data. *Bioinformatics*. 2010;26(1):139–140. doi: [10.1093/bioinformatics/btp616](https://doi.org/10.1093/bioinformatics/btp616)
 26. Metsalu T, Vilo J. ClustVis: a web tool for visualizing clustering of multivariate data using Principal Component Analysis and heatmap. *Nucleic Acids Res*. 2015;43(W1):W566–W570. doi: [10.1093/nar/gkv468](https://doi.org/10.1093/nar/gkv468)
 27. Ge SX, Jung D, Yao R. ShinyGO: a graphical gene-set enrichment tool for animals and plants. *Bioinformatics*. 2020;36(8):2628–2629. doi: [10.1093/bioinformatics/btz931](https://doi.org/10.1093/bioinformatics/btz931)
 28. Ewels P, Magnusson M, Lundin S, Källér M. MultiQC: summarize analysis results for multiple tools and samples in a single report. *Bioinformatics*. 2016;32(19):3047–3048. doi: [10.1093/bioinformatics/btw354](https://doi.org/10.1093/bioinformatics/btw354)
 29. Freund A, Laberge RM, Demaria M, Campisi J. Lamin B1 loss is a senescence-associated biomarker. *Mol Biol Cell*. 2012;23(11):2066–2075. doi: [10.1091/mbc.E11-10-0884](https://doi.org/10.1091/mbc.E11-10-0884)
 30. Tracz MJ, Alam J, Nath KA. Physiology and pathophysiology of heme: implications for kidney disease. *J Am Soc Nephrol*. 2007;18(2):414–420. doi: [10.1681/ASN.2006080894](https://doi.org/10.1681/ASN.2006080894)
 31. Nath KA. Heme oxygenase-1 and acute kidney injury. *Curr Opin Nephrol Hypertens*. 2014;23(1):17–24. doi: [10.1097/01.mnh.0000437613.88158.d3](https://doi.org/10.1097/01.mnh.0000437613.88158.d3)
 32. Harris AS, Aratani S, Johmura Y, Suzuki N, Dan L, Nakanishi M. In vivo dynamics of senescence in rhabdomyolysis-induced acute kidney injury. *Biochem Biophys Res Commun*. 2023;673:121–130. doi: [10.1016/j.bbrc.2023.06.046](https://doi.org/10.1016/j.bbrc.2023.06.046)
 33. Li C, Shen Y, Huang L, Liu C, Wang J. Senolytic therapy ameliorates renal fibrosis postacute kidney injury by alleviating renal senescence. *FASEB J*. 2021;35(1):e21229. doi: [10.1096/fj.202001855RR](https://doi.org/10.1096/fj.202001855RR)
 34. Li S, Livingston MJ, Ma Z, et al. Tubular cell senescence promotes maladaptive kidney repair and chronic kidney disease after cisplatin nephrotoxicity. *JCI Insight*. 2023;8(8):e166643. doi: [10.1172/jci.insight.166643](https://doi.org/10.1172/jci.insight.166643)
 35. Yang L, Besschetnova TY, Brooks CR, Shah JV, Bonventre JV. Epithelial cell cycle arrest in G2/M mediates kidney fibrosis after injury. *Nat Med*. 2010;16(5):535–543. doi: [10.1038/nm.2144](https://doi.org/10.1038/nm.2144)
 36. Hedblom A, Hejazi SM, Canesin G, et al. Heme detoxification by heme oxygenase-1 reinstates proliferative and immune balances upon genotoxic tissue injury. *Cell Death Dis*. 2019;10(2):72. doi: [10.1038/s41419-019-1342-6](https://doi.org/10.1038/s41419-019-1342-6)
 37. Gonzalez-Michaca L, Farrugia G, Croatt AJ, Alam J, Nath KA. Heme: a determinant of life and death in renal tubular epithelial cells. *Am J Physiol Renal Physiol*. 2004;286(2):F370–F377. doi: [10.1152/ajprenal.00300.2003](https://doi.org/10.1152/ajprenal.00300.2003)
 38. Nath KA, Hebbel RP. Sick cell disease: renal manifestations and mechanisms. *Nat Rev Nephrol*. 2015;11(3):161–171. doi: [10.1038/nrneph.2015.8](https://doi.org/10.1038/nrneph.2015.8)
 39. Suvakov S, Ghamrawi R, Cubro H, et al. Epigenetic and senescence markers indicate an accelerated ageing-like state in women with preeclamptic pregnancies. *EBioMedicine*. 2021;70:103536. doi: [10.1016/j.ebiom.2021.103536](https://doi.org/10.1016/j.ebiom.2021.103536)
 40. Tolosano E, Hirsch E, Patrucco E, et al. Defective recovery and severe renal damage after acute hemolysis in hemopexin-deficient mice. *Blood*. 1999;94(11):3906–3914. doi: [10.1182/blood.v94.11.3906](https://doi.org/10.1182/blood.v94.11.3906)
 41. Gentinetta T, Belcher JD, Brügger-Verdon V, et al. Plasma-derived hemopexin as a candidate therapeutic agent for acute vaso-occlusion in sickle cell disease: preclinical evidence. *J Clin Med*. 2022;11(3):630. doi: [10.3390/jcm11030630](https://doi.org/10.3390/jcm11030630)
 42. Fan X, Zhang X, Liu LC, et al. Hemopexin accumulates in kidneys and worsens acute kidney injury by causing hemoglobin deposition and exacerbation of iron toxicity in proximal tubules. *Kidney Int*. 2022;102(6):1320–1330. doi: [10.1016/j.kint.2022.07.024](https://doi.org/10.1016/j.kint.2022.07.024)